Biosensors and Bioelectrochemistry 186 (2021) 113263

Contents lists available at ScienceDirect

Biosensors and Bioelectronics

journal homepage: www.elsevier.com/locate/bios

Ultrasensitive ratiometric electrochemiluminescence for detecting *atxA* mRNA using luminol-encapsulated liposome as effectively amplified signal labels

Si Yu Xiao [a], Shu Jun Zhen [a], Cheng Zhi Huang [b,*], Yuan Fang Li [a,**]

[a] Key Laboratory of Luminescence Analysis and Molecular Sensing (Southwest University), Ministry of Education, College of Chemistry and Chemical Engineering, Southwest University, Chongqing, 400715, PR China

[b] Key Laboratory of Luminescent and Real-Time Analytical System (Southwest University), Chongqing Science and Technology Bureau, College of Pharmaceutical Sciences, Southwest University, Chongqing, 400715, PR China

ARTICLE INFO

Keywords:
Electrochemiluminescence
Ratiometric biosensor
Silver metal-organic gel
Liposome
Dissolved oxygen

ABSTRACT

It is an advantageous way to quickly identify the toxicity of *Bacillus anthracis* (*B. anthracis*) by detecting the transcription product of the *atxA* gene. Herein, a novel ultrasensitive ratiometric electrochemiluminescence (ECL) biosensor with competitive mechanism and double amplified signal ways was proposed for detecting the *atxA* mRNA. The $K_2S_2O_8$ was used as cathodic emitter and silver metal-organic gels (AgMOG) was used as ECL enhancer. The AgMOG could accelerate the electro-catalytic reduction of $S_2O_8^{2-}$ to $SO_4^{\cdot-}$, which reacted with dissolved oxygen, resulting in strong cathodic ECL. Meanwhile, luminol was encapsulated in liposome as anodic amplified signal labels and the luminol anion radical also reacted with dissolved oxygen to create the anodic ECL emission. We immobilized luminol-encapsulated liposomes on the surface of AgMOG through the hybridization of DNA and mRNA. This would provide a competitive mechanism involving dissolved oxygen between $K_2S_2O_8$ and luminol. Benefiting from the competitive mechanism and amplified signal ways, this ratiometric biosensor achieved a wide linear relationship range from 10 to 300 fM with a low limit of detection (8.13 fM). Considering the accessible operation, favorable performance, and high universality of this strategy, this work may be used to analyze other mRNAs of bacteria.

1. Introduction

Bacillus anthracis (*B. anthracis*), as a spore-forming and Gram-positive bacterium, can cause the potentially fatal disease anthrax. It is very important to quickly identify *B. anthracis* because it could be used as a biological weapon by terrorists (Hartley and Baeumner, 2003). However, it is time-consuming to identify *B. anthracis* based on phenotypic characteristics of the bacteria (Edwards and Baeumner, 2006c). Therefore, it is an advantage to develop a nucleotide-based system for quickly detecting any strain of *B. anthracis*.

To achieve sensitive detection of nucleic acids, many works focus on developing a variety of analytical techniques, including colorimetry (Hosseinzadeh et al., 2018), fluorescence (Smith et al., 2018; Xia et al., 2018), electrochemistry (Miao et al., 2018; Yu et al., 2018), electrochemiluminescence (ECL) (Li et al., 2019a; Liu et al., 2017; Zhou et al., 2018), etc. Among the proposed methodologies, ECL is an ideal technique to detect nucleic acid with low background, high sensitivity and wide linear ranges (Li et al., 2019b). However, it is still a challenge to achieve ultrasensitive detection of mRNA due to its low abundance in cells and strong sequence homology with other irrelevant mRNAs (Wang et al., 2020). Researchers focus on immobilizing more signal labels on the electrode surface with nanomaterial as carrier to enhance the sensitivity and lower the limit of detection, such as silica (Liang et al., 2015), liposomes (Qi et al., 2013), quantum dots (Carrara et al., 2017), noble metal clusters (Wang et al., 2018), and 3D metal-organic frameworks (Xiong et al., 2017). Especially, liposomes are highly versatile lipid bilayer structures with a hollow cavity. Nanoparticles or molecules can be embedded in cavities or immobilized on the surface of liposomes through covalent or non-covalent interactions, which leads to a variety of applications such as drug delivery (Liu et al., 2020) and fluorescence

* Corresponding author.
** Corresponding author.
E-mail addresses: chengzhi@swu.edu.cn (C.Z. Huang), liyf@swu.edu.cn (Y.F. Li).

https://doi.org/10.1016/j.bios.2021.113263
Received 23 February 2021; Received in revised form 12 April 2021; Accepted 16 April 2021
Available online 1 May 2021

assays (Ma et al., 2019). Moreover, liposomes have many advantages in biosensor applications due to their biocompatibility and high carrying capacity properties (Trapani et al., 2018). A signal enhancement of up to several orders of magnitude can be obtained since a large number of reporter molecules in liposomes (Edwards and Baeumner, 2006a). Therefore, the combination of ECL and liposomes will provide great advantages (Mayer et al., 2018).

Although many ECL biosensors have been proposed with signal amplification to achieve satisfactory sensitivity, the biosensors constructed based on single-signal strategies will inevitably have false positive or false negative errors due to the influence of the instrumental or some environmental factors (Ying et al., 2017). The double signal-based construction strategies will be a superior choice to solve the above problems (Wang et al., 2020; Zhang et al., 2020). The ratiometric biosensor will provide the final detecting outputs as the relative intensity of two different luminescent signals due to their dual-emission-center structure. Such a self-calibrating mechanism greatly minimizes the influence of external conditions and exhibits promising sensing capabilities with respect to analytes, such as high accuracy and sensitivity, making ratiometric biosensors capable in more realistic and complicated environments (Guo et al., 2020).

The luminol and $K_2S_2O_8$ show great advantages as double ECL signal emitters due to the potential-resolved and maximum emission wavelength-resolved property (Zhang et al., 2016). The maximum ECL emission wavelengths of $K_2S_2O_8$ are at 525 and 620 nm (Xiao et al., 2020; Yao et al., 2008) and that of luminol is about 430 nm (Huo et al., 2018; Shao et al., 2016). The ratiometric ECL biosensor can be fabricated based on the maximum emission wavelength-resolved property of emitters (Fan et al., 2020; Zhu et al., 2019). Moreover, the ECL emission potential of $K_2S_2O_8$ and luminol are at the cathode and anode, respectively (Huang et al., 2016; Mayer et al., 2018; Niu et al., 2011; Wang et al., 2016). Therefore, the ratiometric ECL biosensor also can be fabricated based on the potential-resolved property. However, it is still a challenge to immobilize luminol on electrode interface. It is a good way to immobilize luminol by encapsulating luminol in liposomes. And the surface of liposomes can be modified by a variety of bio-recognition elements, such as DNA. Then, it can be further connected to the electrode surface. In addition, the ECL intensity of $K_2S_2O_8$ is too weak which limits its application. Recently, a novel silver metal-organic gel (AgMOG) has been reported for the first time as the promising ECL enhancer of $K_2S_2O_8$ because of their advantages of easy preparation and strong ECL enhancement (Xiao et al., 2020).

The virulence of *B. anthracis* results from the production of the toxin consists of three proteins whose expression requires the transcription products of *atxA* gene (Bongiorni et al., 2008). *AtxA* positively regulates the expression of these three toxin genes (Corsi et al., 2021). The toxicity of *B. anthracis* enhances with more transcription products of *atxA* gene (Bertin et al., 2010). Therefore, the pathogenic bacteria can be quickly identified by determining whether the *atxA* gene of *B. anthracis* is transcribed. Herein, we proposed the dual-signal ratiometric ECL biosensor for *atxA* mRNA detection, as illustrated in Scheme 1. The AgMOG could accelerate the electro-catalytic reduction of $S_2O_8^{2-}$ to $SO_4^{\cdot-}$ which reacted with dissolved oxygen, resulting in cathodic ECL. Meanwhile, the luminol anion radical also reacted with dissolved oxygen, creating the anodic ECL emission. In the presence of more *atxA* mRNA, more liposomes were immobilized on the electrode to provide greatly amplified the anodic ECL emission. Then, the dissolved oxygen was consumed and the cathodic ECL emission was weakened. Based on the ratio of ECL intensities at two excitation potentials, the ratiometric ECL biosensor could achieve the ultrasensitive determination of *atxA* mRNA.

2. Experimental

2.1. Preparation of the AgMOG

The preparation of AgMOG was synthesized by a simple one-step mixing method, according to our previous study (Xiao et al., 2020). 0.5 mL of 0.032 M 2,6-Bis(2-benzimidazolyl)pyridine (BBPY) in CH_3OH and 0.5 mL of 0.032 M $AgNO_3$ in deionized water were added into the eppendorf (EP) tube. After intensive mixing, the mixture was placed for 30 min at room temperature to obtaine the AgMOG. Then, the AgMOG was dried by freeze-drying treatment and the dried AgMOG was dispersed in deionized water for further use.

2.2. Preparation of luminol-encapsulated liposomes

Luminol-encapsulated liposomes were prepared according to the literature with slight modifications (Men et al., 2018). 19.8 mg L-α-Phosphatidylcholine (PC), 7.6 mg 1,2-Distearoyl-*sn-glycero*-3-phosphoethanolamine-N-[methoxy-(polyethyleneglycol)-2000] (DSPE-PEG) and 4.76 mg cholesterol were added into 1 mL chloroform in a round-bottom flask. Then, the chloroform was removed using a rotary evaporator at 40 °C under reduced pressure for 30 min to obtain a thin lipid film and the flask was placed under vacuum drying for 6 h to remove residual organic solvent traces. Subsequently, 1 mL phosphate buffer saline (PBS) (0.1 M, pH 8.0)

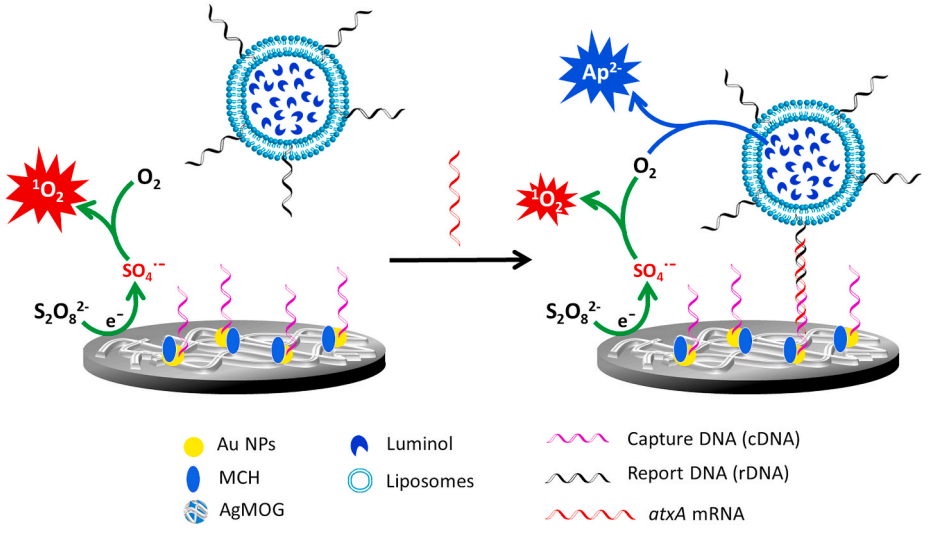

Scheme 1. Schematic representation of the AgMOG enhanced $K_2S_2O_8$ and luminol-encapsulated in liposomes competitive-mechanism-driven ECL biosensor for ratiometric detection of *Atxa* mRNA.

containing 20 mM luminol was added in the thin lipid film for 1 h with vigorous shaking at 37 °C to form liposomes. Then, the liposome was passed through the 0.4 μm polycarbonate film. The untapped luminol was removed by a dialysis bag with 300 kDa molecular weight cut off (MWCO) at 4 °C in PBS with stirring for 24 h. The obtained liposomes were stored at 4 °C for further use. All operations after adding luminol to the thin lipid film are completed in the absence of light.

2.3. Preparation of the rDNA-liposomes hybrid probe

In short, 200 μL of liposomes and 200 μL of report DNA probe (rDNA) modified with cholesterol in 0.01 M PBS (pH 7.4) were added into 1.5 mL EP with vigorous shaking at 37 °C for 2 h. Then, the unbound rDNA probe was removed and washed with 0.01 M PBS. The obtained rDNA-liposomes hybrid probe was stored at 4 °C for further use.

2.4. Native polyacrylamide gel electrophoresis (PAGE)

The target DNA (tDNA) was added into the mixtures of 5 μM capture DNA (cDNA) and rDNA, and incubated in reaction buffer for 2 h. The different samples were carefully added to the lanes of gel electrophoresis (the preparation process was described in Supporting Information) after mixing with the loading buffer, respectively. After electrophoresis which was run at 110 V for about 60 min, the gel was stained in ethidium bromide (EB) solution for 15 min. Finally, the electrophoresis photo after staining was obtained by photographing under UV light.

2.5. Construction of the biosensor and analysis procedure

The glassy carbon electrode (GCE) was polished with alumina powder and washed to obtain the mirror-like surface. Then, 5 μL of AgMOG and 5 μL of Au NPs solutions were dropped onto the pretreated electrodes surface and dried naturally in air, respectively. Next, 5 μL of 2 μM thiolated cDNA was dripped onto the modified electrode and incubated overnight. Then 6-mercapto-1-hexanol (MCH) was used to block non-specific sites for 2 h. Subsequently, 5 μL of tDNA was added to the electrode and incubated for 2 h. Then, 5 μL of the rDNA-liposomes hybrid probe was dropped to the prepared electrodes and incubated for 1 h. The electrode was rinsed with buffer solution after each step. At last, the constructed biosensor was detected in PBS (0.1 M, pH 7.4) containing 10 mM $K_2S_2O_8$ from −2 to 0.4 V.

3. Results and discussion

3.1. Characterization of the AgMOG and luminol-encapsulated liposomes

The microscopic morphology of this facile one-step synthetic AgMOG was observed by scanning electron microscopy (SEM). The fiber structure with a diameter of about 50 nm and a length of several micrometers was observed (Fig. 1A). Next, the viscoelastic property of this gel was characterized by rheology investigation (Fig. 1B). The typical storage modulus (G′) and loss modulus (G″) vs. frequency curves of AgMOG showed that G′ and G″ are almost independent frequencies and G′ was greater than G″ at any given point, indicating that a real gel material was formed which was consistent with the visually observable inverted phenomenon (Fig. 1B, insert). These results indicated the successful synthesis of AgMOG material.

To investigate the successful preparation of luminol-encapsulated liposomes, the transmission electron microscopy (TEM) and ultraviolet visible (UV–vis) absorption were measured. As shown in Fig. 1C, the TEM image showed that the as-fabricated liposomes appeared as quasi-spherical vesicles. The UV–vis absorption spectra of liposomes showed the typical luminol absorption peak at 300 nm and 350 nm (Fig. 1D). Furthermore, the atomic force microscopy (AFM) image (Fig. S1) showed that the as-fabricated liposomes appeared as a height of 20 ± 1 nm and a lateral dimension of ~200 nm corresponding to the adsorbed,

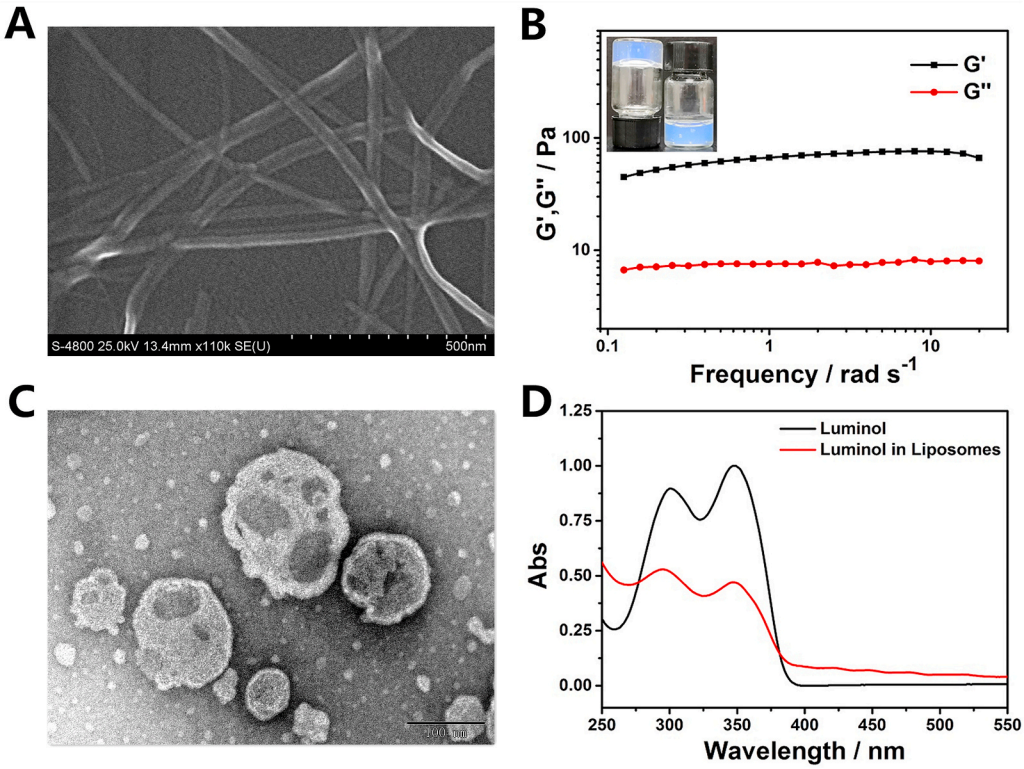

Fig. 1. Characterization of AgMOG and luminol-encapsulated liposomes. (A) SEM image of AgMOG. (B) Plot of storage modulus (G′) and loss modulus (G″) of AgMOG. The insert picture is the photograph of AgMOG. (C) TEM image of luminol-encapsulated liposomes. (D) The UV–vis absorption spectra of luminol-encapsulated liposomes.

flattened vesicles, similarly to what was previously reported (Angayarkanni et al., 2019; Ye et al., 2020). In the light of these facts, the luminol-encapsulated liposomes were synthesized successfully.

3.2. Feasibility of DNA hybridization assay

The sequences of the nucleic acids were listed in Table S1. In addition to the natural *atxA* mRNA, a synthetic target sequence was designed which facilitated the development of the biosensor. The first 20 bases and final 21 bases are complementary to the rDNA and cDNA, respectively. The red "TC" was selected to link the two sequences because it created a DNA sequence with minimal hypothetical secondary structure (Hartley and Baeumner, 2003).

The prepared samples of different hybridization assay were carried out by a PAGE experiment to assess the feasibility of the hybridization reaction. By comparing lane 2 (cDNA + tDNA) with lane 5 (cDNA) and lane 6 (tDNA) in the gel electrophoresis photo (Fig. 2), there was a bright band on the upper part of lane 2 and the band of cDNA was undiscovered on the lane 2, indicating that the cDNA and tDNA could hybridize with each other. By comparing lane 3 (rDNA + tDNA) with lane 6 (tDNA) and lane 7 (rDNA), a bright band appeared at the top of lane 3, indicating that the rDNA and tDNA could hybridize with each other. By comparing lane 4 (cDNA + rDNA) with lane 5 (cDNA) and lane 7 (rDNA), no obvious band appeared at the top of lane 4, indicating that the cDNA and rDNA could not hybridize with each other. Moreover, the lane 1 (cDNA + tDNA + rDNA) showed three bright bands and the band at the top indicated that cDNA, tDNA and rDNA could form a larger DNA structure. Overall, the PAGE experiment indicated the DNA hybridization was successful.

3.3. Characterization of the biosensor

The particle size distribution (Fig. 3A) and zeta potential (Fig. 3A, insert) of the liposomes and liposomes modified with rDNA were measured to prove the successful attachment of DNA to the liposomes. The hydrodynamic diameters of liposomes with rDNA and liposomes without any modification were about 121 nm and 116 nm, respectively. The hydrodynamic diameter of liposomes modified with rDNA was slightly larger than that of unmodified liposomes (Fang et al., 2020). In addition, after the modification with rDNA, the zeta potential of liposomes was changed from −3.77 mV to −5.54 mV due to negative charge of the DNA (Wang et al., 2019). The changes of size and zeta potential implied that cDNA was connected to the liposomes successfully.

The assembly process of the ECL biosensor was characterized via electrochemical impedance spectroscopy (EIS), cyclic voltammetry (CV) and ECL. As shown in Fig. 3B, the impedance value of the AgMOG modified electrode was decreased obviously (curve b) compared with the bare GCE electrode (curve a) because of the good conductivity of AgMOG (Xiao et al., 2020). When Au NPs was connected to the surface of the AgMOG, the electron transfer resistance further decreased (curve c) because Au NPs could accelerate electron transfer. After reacting with cDNA and MCH, the electron transfer resistance increased significantly (curve d), since MCH could suppress electron transfer on the electrode. However, when the rDNA-liposomes were connected to the surface of the electrode surface by bonding with the target sequence DNA and cDNA, the charge transfer resistance reduced (curve e). This was ascribed to the hydrophilicity and rigidity of the DNA duplex that caused DNA to reside further from the electrode surface and facilitate the approach of negatively charged redox moieties to the interface (Han et al., 2019).

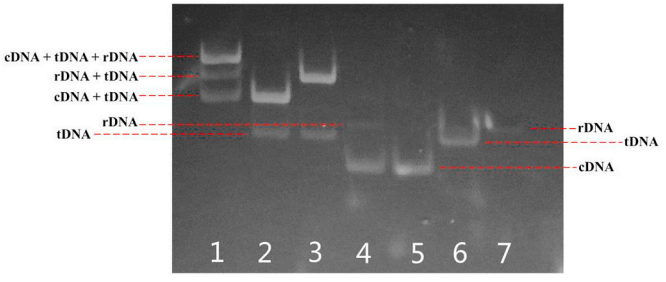

Fig. 2. PAGE (12%) analysis of the DNA hybridization reaction. lane 1, cDNA (5 μM) + tDNA (5 μM) + rDNA (5 μM); lane 2, cDNA (5 μM) + tDNA (5 μM); lane 3, tDNA (5 μM) + rDNA (5 μM); lane 4, cDNA (5 μM) + rDNA (5 μM); lane 5, cDNA (5 μM); lane 6, tDNA (5 μM); lane 7, rDNA (5 μM).

To further confirm the fabrication process of the modified electrode, the CVs were also performed in $Fe(CN)_6^{3-/4-}$ solution. As shown in Fig. S2, a pair of clear redox peaks could be observed at bare GCE (curve a). After modifying AgMOG on the electrode surface, the redox peak current increased relatively (curve b) because of the good conductivity of AgMOG. The peak current increased continuatively after Au NPs were assembled on the electrode surface (curve c). This was because Au NPs could accelerate the electron transfer between the $Fe(CN)_6^{4-/3-}$ and the electrode. After modifying cDNA and MCH were successively modified onto the electrode (curves d), the redox peak currents obviously decreased due to the insulation of MCH. However, when tDNA and rDNA-liposomes were connected on the electrode surface (curve e), the redox peak current was increased significantly. This could be attributed to the rigidity of the DNA duplex, resulting in the easy approach of Fe $(CN)_6^{4-/3-}$ to the interface (Pan and Rothberg, 2005).

Meanwhile, the ECL responses of three different modified GCE were measured and shown in Fig. S3. There was only a strong cathode ECL peak of AgMOG/GCE (curve a) from $K_2S_2O_8$. After the modification of cDNA and MCH on GCE, the cathode ECL emission decreased (curve b) because the MCH decreased the electron transfer rate. Then, the luminol-encapsulated liposomes were linked to GCE via tDNA and there were a strong anodic ECL peak from luminol and a weaker cathode ECL peak from $K_2S_2O_8$ (curve c), suggesting the feasibility of this dual-emission ECL ratiometric biosensor for nucleic acid assay. Therefore, all of the above results demonstrated that the ECL biosensor was constructed successfully.

3.4. ECL mechanism of the biosensor

When the potential was scanned in the negative direction to −2.0 V, the $K_2S_2O_8$ was electrochemically reduced to $SO_4^{\bullet-}$ and the AgMOG could accelerate the reduction of $S_2O_8^{2-}$ to generate more $SO_4^{\bullet-}$ (Lei et al., 2018; Xiao et al., 2020). At the same time, the dissolved oxygen was reduced to $HOO^{\bullet}$. Then the strong oxidant $SO_4^{\bullet-}$ could react with the $HOO^{\bullet}$ to produce $^1(O_2)_2$* as light-emitting species, producing a strong ECL signal. When the potential was scanned to 0.4 V, the large amounts of luminol could deprotonate to form intermediate oxidation state of luminol ($L^{\bullet-}$) and the $L^{\bullet-}$ could react with dissolved oxygen to produced $O_2^{\bullet-}$ radicals. Then the $L^{\bullet-}$ radicals reacted with the $O_2^{\bullet-}$ radicals to generate the excited state of 3-aminophthalate (Ap^{2-}*) for ECL emission (Gu et al., 2020). The possible mechanism of reaction was outlined as follows:

Under cathode potential:

$$S_2O_8^{2} + e^{-} \xrightarrow{AgMOG} SO_4^{2-} + SO_4^{-} \quad (1)$$

$$O_2 + H_2O + e^{-} \rightarrow HOO^{\cdot} + HO^{-} \quad (2)$$

$$SO_4^{-} + HOO^{\cdot} \rightarrow HSO_4^{-} + {}^1(O_2)_2{}^* \quad (3)$$

$$^1(O_2)_2{}^* \rightarrow 2\,^3O_2 + h\nu \quad (4)$$

Under anodic potential:

$$HL^{-} - e^{-} \rightarrow L^{\bullet-} + H^{+} \quad (5)$$

$$L^{\bullet-} + O_2 \rightarrow L + O_2^{\bullet-} \quad (6)$$

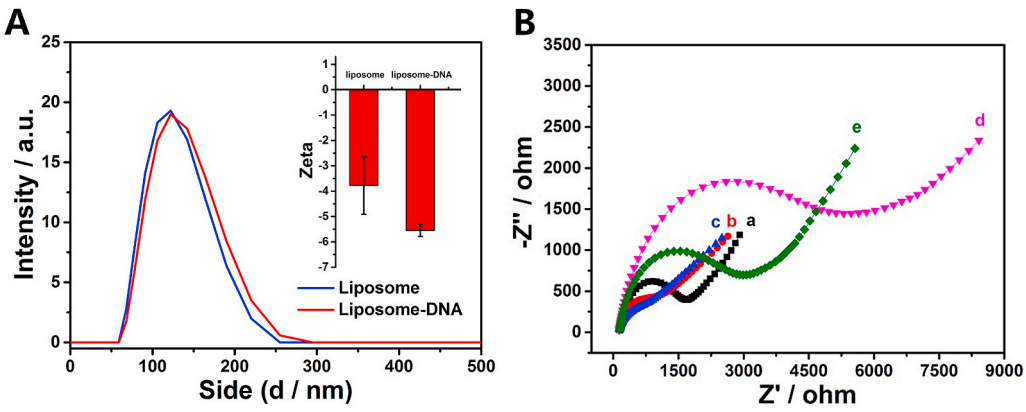

Fig. 3. Characterization of the biosensor. (A) The size distribution of luminol-encapsulated liposomes (blue line), and liposomes modified with DNA (red line). The insert: the zeta potential of liposomes and liposomes modified with DNA. (B) The EIS at the (a) bare GCE; (b) AgMOG/GCE; (c) AuNPs/AgMOG/GCE; (d) MCH/DNA/AuNPs/AgMOG/GCE; (e) Liposomes/MCH/DNA/AuNPs/AgMOG/GCE in 5.0 mM $[Fe(CN)_6]^{3-/4-}$. (For interpretation of the references to color in this figure legend, the reader is referred to the Web version of this article.)

$$L^{\bullet -} + O_2^{\bullet -} \rightarrow LO_2^{2-} \quad (7)$$

$$LO_2^{2-} \rightarrow Ap^{2-}* + N_2 \quad (8)$$

$$Ap^{2-}* \rightarrow Ap^{2-} + h\nu \quad (9)$$

Based on the above, dissolved oxygen was used as the co-reactant of both $K_2S_2O_8$ and luminol. The influence of dissolved oxygen was confirmed with the experiment of removing dissolved oxygen from the solution prepared by boiling water (Fig. S4). The ECL intensity of $K_2S_2O_8$ and luminol was decreased after removing dissolved oxygen indicating that oxygen was involved in the process of cathodic and anodic ECL generation.

The intensity of ECL increases with the number of illuminant. When the amount of tDNA increased, more luminol-encapsulated liposomes will be immobilized on the electrode, resulting in the increased anodic ECL intensity. On the one hand, the luminescence of luminol would consume a large amount of dissolved oxygen, resulting in the reducing of dissolved oxygen which further weakened the ECL of $K_2S_2O_8$. On the other hand, liposomes could hinder the contact of $K_2S_2O_8$ and AgMOG, and reduce the catalytic effect of AgMOG, resulting in weakening ECL of $K_2S_2O_8$. Therefore, when the amount of target nucleic acid was more, the ECL emission of luminol was stronger and the ECL emission of $K_2S_2O_8$ was weaker.

3.5. Ratiometric detection of atxA mRNA

To obtain favorable detection results, several interrelated factors including the concentration of AgMOG, $K_2S_2O_8$, and the incubation time of the report DNA-liposomes hybrid probe on the electrodes were optimized. The suitable concentration of AgMOG was 1.5 mg/mL (Fig. S5). The best concentration of $K_2S_2O_8$ was 10 mM (Fig. S6). The excellent incubation time of the report DNA-liposomes hybrid probe on the electrodes was 60 min (Fig. S7).

Under the optimal conditions, with the increasing concentration of *atxA* mRNA, the ECL_a (the anodic ECL) intensity of luminol exhibited a gradual enhancement and the ECL_c (the cathode ECL) intensity of $K_2S_2O_8$ exhibited a gradual decrease simultaneously (Fig. 4A), which indicated the good capability of the biosensor in response to the target. The relationship between the ECL_a/ECL_c intensity and the concentration of *atxA* mRNA was described as the linear regression equation of $ECL_a/ECL_c = 0.0241c - 0.194$, where c symbolized for the *atxA* mRNA concentration from 10 to 300 fM, $R^2 = 0.990$ (Fig. 4B). The limit of detection (LOD) was calculated as 8.13 fM by the ratio of 3σ to K, where σ was the standard deviation of the blank measurements (n = 10) and K was the slope of the corresponding linear regression equation. Obviously, this dual signal mode exhibits high sensitivity and a good linear correlation, demonstrating great superiority of the ratiometric ECL biosensor.

Compared to previously reported *atxA* mRNA detection systems, our ratiometric ECL biosensor displayed comparable or even better sensitivity (Table S2). Moreover, as far as we know, this is the first time that ECL platform was used to detect *atxA* mRNA. Although some previous biosensors were based on liposomes as signal-amplified labels (Baeumner et al., 2004; Edwards and Baeumner, 2006b; Edwards et al., 2008; Hartley and Baeumner, 2003), there is no doubt that ECL-based biosensors are more sensitive.

The stability and reproducibility are important to the obtained ECL biosensor. The stability of the biosensor was investigated under consecutive scanning for six cycles with 200 fM *atxA* mRNA (Fig. S8). Those responses almost kept constant with RSDs of the cathode ECL and the anodic ECL as low as 4.59% and 1.55%, respectively. Moreover, we independently prepared five modified electrodes with 100 fM *atxA* mRNA under the same conditions to investigate the reproducibility (Fig. S9). The obtained ECL signals showed no significant change and the RSDs of the cathode ECL and the anodic ECL were 6.33% and 3.22%

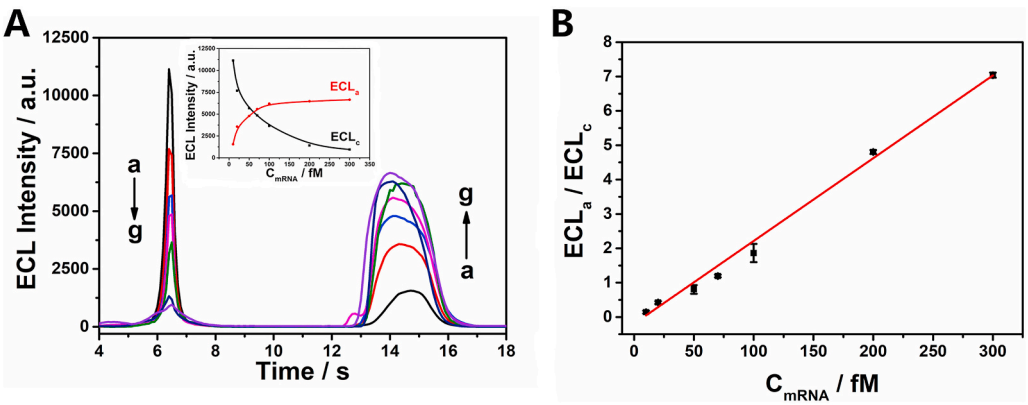

Fig. 4. Ratiometric detection of *atxA* mRNA. (A) ECL-time curves of the modified electrode at different concentrations of *atxA* mRNA (a–g: 10, 20, 50, 70, 100, 200 and 300 fM) recorded in pH 7.4 PBS solution containing 10 mM $K_2S_2O_8$. Inset A: relationships of ECL_a (red line) and ECL_c (black line) with different concentrations of *atxA* mRNA. (B) The calibration plots between ECL_a/ECL_c and the concentrations of *atxA* mRNA. (For interpretation of the references to color in this figure legend, the reader is referred to the Web version of this article.)

respectively, meaning an acceptable reproducibility.

The selectivity of the ratiometric ECL biosensor for *atxA* mRNA was investigated in the presence of glucose (Glu), sodium of ascorbic acid (AA), glutathione (GSH), bovine serum albumin (BSA), and the experimental results showed that *atxA* mRNA could induce the most changes in the ECL intensity (Fig. S10). Therefore, *atxA* mRNA could be selectively detected by the ratiometric ECL biosensor. Moreover, we used Escherichia coli (*E. coli*) as the model bacterium to detect the actual sample by standard addition method. The *E. coli* was cultured in liquid medium to obtain bacteria in logarithmic growth phase. Then, the RNA of *E. coli* was extracted by using the Bacteria Total RNA Isolation Kit for detecting the actual sample. As shown in Table S3, the biosensor showed a good recovery rate. Therefore, it had potential applications in analysis of real samples.

4. Conclusions

In summary, a ratiometric ECL biosensor was designed for the detection of *atxA* mRNA using luminol-encapsulated liposome as effectively amplified signal labels. On the one hand, as an effective ECL enhancer, the AgMOG could enhance the ECL emission of $K_2S_2O_8$ as the cathode ECL. On the other hand, the luminol-encapsulated liposome could provide a superior anodic ECL signal. This ratiometric ECL biosensor possessed a competitive mechanism involving the dissolved oxygen between $K_2S_2O_8$ and luminol. There is no doubt that this can greatly improve the sensitivity of the ratiometric ECL biosensor. Different from the traditional biosensors constructed based on single-signal strategies, this novel ratiometric biosensor offered both high sensitivity and credibility. The results of this work manifested that the proposed ratiometric ECL biosensor held promising potential capabilities to identify *B. anthracis*. Furthermore, this typical competitive ECL mechanism involving dissolved oxygen would provide new prospects for further advance of highly sensitive ECL detection systems.

CRediT authorship contribution statement

Si Yu Xiao: Conceptualization, Methodology, Investigation, Data curation, Validation, Formal analysis, Analysis, Writing – original draft. **Shu Jun Zhen:** Writing – review & editing. **Cheng Zhi Huang:** Formal analysis, Writing – review & editing. **Yuan Fang Li:** Funding acquisition, Formal analysis, Writing – review & editing, Project administration.

Declaration of competing interest

The authors declare that they have no known competing financial interests or personal relationships that could have appeared to influence the work reported in this paper.

Acknowledgement

This study was supported by the National Natural Science Foundation of China (NSFC, No. 21874109).

Appendix A. Supplementary data

Supplementary data to this article can be found online at https://doi.org/10.1016/j.bios.2021.113263.

References

Angayarkanni, S.A., Kampf, N., Klein, J., 2019. Langmuir 35 (48), 15469–15480.
Baeumner, A.J., Leonard, B., McElwee, J., Montagna, R.A., 2004. Anal. Bioanal. Chem. 380 (1), 15–23.
Bertin, M., Château, A., Fouet, A., 2010. Res. Microbiol. 161 (4), 249–259.
Bongiorni, C., Fukushima, T., Wilson, A.C., Chiang, C., Mansilla, M.C., Hoch, J.A., Perego, M., 2008. J. Bacteriol. 190 (19), 6483–6492.
Carrara, S., Arcudi, F., Prato, M., DeCola, L., 2017. Angew. Chem. Int. Ed. 56 (17), 4757–4761.
Corsi, I.D., Dutta, S., van Hoof, A., Koehler, T.M., 2021. Front. Microbiol. 11.
Edwards, K.A., Baeumner, A.J., 2006a. Talanta 68 (5), 1421–1431.
Edwards, K.A., Baeumner, A.J., 2006b. Anal. Bioanal. Chem. 386 (6), 1613–1623.
Edwards, K.A., Baeumner, A.J., 2006c. Anal. Chem. 78 (6), 1958–1966.
Edwards, K.A., Curtis, K.L., Sailor, J.L., Baeumner, A.J., 2008. Anal. Bioanal. Chem. 391 (5), 1689–1702.
Fan, Z., Lin, Z., Wang, Z., Wang, J., Xie, M., Zhao, J., Zhang, K., Huang, W., 2020. ACS Appl. Mater. Interfaces 12 (10), 11409–11418.
Fang, C., Deng, Z., Cao, G.D., Chu, Q., Wu, Y.L., Li, X., Peng, X.S., Han, G.R., 2020. Adv. Funct. Mater. 30 (16), 1910085.
Gu, W.L., Wang, H.J., Jiao, L., Wu, Y., Chen, Y.X., Hu, L.Y., Gong, J.M., Du, D., Zhu, C.Z., 2020. Angew. Chem. Int. Ed. 59 (9), 3534–3538.
Guo, X.L., Zhu, N.S., Lou, Y., Ren, S.Y., Pang, S.R., He, Y.Q., Chen, X.B., Shi, Z., Feng, S. H., 2020. Chem. Commun. 56 (40), 5389–5392.
Han, Z.L., Shu, J.N., Liang, X., Cui, H., 2019. Anal. Chem. 91 (19), 12260–12267.
Hartley, H.A., Baeumner, A.J., 2003. Anal. Bioanal. Chem. 376 (3), 319–327.
Hosseinzadeh, E., Ravan, H., Mohammadi, A., Mohammad-rezaei, R., Norouzi, A., Hosseinzadeh, H., 2018. Biosens. Bioelectron. 117, 567–574.
Huang, Y., Lei, J., Cheng, Y., Ju, H., 2016. Biosens. Bioelectron. 77, 733–739.
Huo, X.-L., Zhang, N., Yang, H., Xu, J.-J., Chen, H.-Y., 2018. Anal. Chem. 90 (22), 13723–13728.
Lei, Y.M., Wen, R.X., Zhou, J., Chai, Y.Q., Yuan, R., Zhuo, Y., 2018. Anal. Chem. 90 (11), 6851–6858.
Li, Y., He, L., Huang, C.Z., Li, Y.F., 2019a. Biosens. Bioelectron. 134, 29–35.
Li, Y., Huang, C.Z., Li, Y.F., 2019b. Anal. Chem. 91 (14), 9308–9314.
Liang, W.B., Zhuo, Y., Xiong, C.Y., Zheng, Y.N., Chai, Y.Q., Yuan, R., 2015. Anal. Chem. 87 (24), 12363–12371.
Liu, Q., Ma, C., Liu, X.P., Wei, Y.P., Mao, C.J., Zhu, J.J., 2017. Biosens. Bioelectron. 92, 273–279.
Liu, X., Wang, P., Zou, Y.-X., Luo, Z.-G., Tamer, T.M., 2020. Food Res. Int. 136, 109587.
Ma, D.F., Xu, C.H., Hou, W.Q., Zhao, C.Y., Ma, J.B., Huang, X.Y., Jia, Q., Ma, L., Diao, J. J., Liu, C., Li, M., Lu, Y., 2019. Angew. Chem. Int. Ed. 58 (17), 5577–5581.
Mayer, M., Takegami, S., Neumeier, M., Rink, S., JacobivonWangelin, A., Schulte, S., Vollmer, M., Griesbeck, A.G., Duerkop, A., Baeumner, A.J., 2018. Angew. Chem. Int. Ed. 57 (2), 408–411.
Men, C., Li, C.H., Wei, X.M., Liu, J.J., Liu, Y.X., Huang, C.Z., Zhen, S.J., 2018. Analyst 143 (23), 5764–5770.
Miao, P., Jiang, Y., Zhang, T., Huang, Y., Tang, Y., 2018. Chem. Commun. 54 (53), 7366–7369.
Niu, H., Yuan, R., Chai, Y.Q., Mao, L., Yuan, Y.L., Zhuo, Y., Yuan, S.R., Yang, X., 2011. Biosens. Bioelectron. 26 (7), 3175–3180.
Pan, S., Rothberg, L., 2005. Langmuir 21 (3), 1022–1027.
Qi, H.L., Qiu, X.Y., Xie, D.P., Ling, C., Gao, Q., Zhang, C.X., 2013. Anal. Chem. 85 (8), 3886–3894.
Shao, K., Wang, B., Ye, S., Zuo, Y., Wu, L., Li, Q., Lu, Z., Tan, X., Han, H., 2016. Anal. Chem. 88 (16), 8179–8187.
Smith, L., Kohli, M., Smith, A.M., 2018. J. Am. Chem. Soc. 140 (42), 13904–13912.
Trapani, A., Mandracchia, D., Tripodo, G., Cometa, S., Cellamare, S., De Giglio, E., Klepetsanis, P., Antimisiaris, S.G., 2018. Colloids Surf., B 170, 11–19.
Wang, H.J., Chai, Y.Q., Li, H., Yuan, R., 2018. Biosens. Bioelectron. 100, 35–40.
Wang, H.Y., Fan, X.X., Wang, Y., 2016. Anal. Bioanal. Chem. 408 (25), 7113–7119.
Wang, J., Haghighatbin, M.A., Shen, W., Mi, L., Cui, H., 2020. Anal. Chem. 92 (10), 7062–7070.
Wang, N.N., Wang, Z.Y., Chen, L.Z., Chen, W.W., Quan, Y.W., Cheng, Y.X., Ju, H.X., 2019. Chem. Sci. 10 (28), 6815–6820.
Xia, Y.K., Wang, L.L., Li, J., Chen, X.Q., Lan, J.M., Yan, A., Lei, Y., Yang, S., Yang, H.H., Chen, J.H., 2018. Anal. Chem. 90 (15), 8969–8976.
Xiao, S.Y., Li, Y., Zhen, S.J., Huang, C.Z., Li, Y.F., 2020. Electrochim. Acta 357, 136842.
Xiong, C.Y., Liang, W.B., Zheng, Y.N., Zhuo, Y., Chai, Y.Q., Yuan, R., 2017. Anal. Chem. 89 (5), 3222–3227.
Yao, W., Wang, L., Wang, H.Y., Zhang, X.L., 2008. Electrochim. Acta 54 (2), 733–737.
Ye, Q.C., Men, C., Li, Y.F., Liu, J.J., Huang, C.Z., Zhen, S.J., 2020. Chem. Commun. 56 (90), 14091–14094.
Ying, Z.M., Wu, Z., Tu, B., Tan, W.H., Jiang, J.H., 2017. J. Am. Chem. Soc. 139 (29), 9779–9782.
Yu, S., Wang, Y.Y., Jiang, L.P., Bi, S., Zhu, J.J., 2018. Anal. Chem. 90 (7), 4544–4551.
Zhang, G.Y., Chai, H.N., Tian, M.W., Zhu, S.F., Qu, L.J., Zhang, X.J., 2020. Anal. Chem. 92 (10), 7354–7362.
Zhang, Q.R., Dai, H., Wang, T., Li, Y.L., Zhang, S.P., Xu, G.F., Chen, S.H., Lin, Y.Y., 2016. Electrochim. Acta 196, 565–571.
Zhou, Y., Wang, H., Zhang, H., Chai, Y., Yuan, R., 2018. Anal. Chem. 90 (5), 3543–3549.
Zhu, L., Ye, J., Yan, M., Zhu, Q., Yang, X., 2019. Analyst 144 (22), 6554–6560.